Manuscript for *Revista Mexicana de Astronomía y Astrofísica* (2007)

CHARACTERIZATION OF A DOUBLE WOLLASTON MODULE FOR POLARIMETRY IN ASTROPHYSICS.

A. García-Pérez,[1] A. Luna,[1] E. O. Serrano-Bernal [1], J. Castro-Ramos,[1] and S. Medina. [2]

Draft version: February 21, 2025

RESUMEN

El módulo Wedge Double Wollaston (WeDoWo) o "doble Wollaston" es un dispositivo capaz de desplegar 4 imágenes de diferente ángulo de polarización (0°, 45°, 90°, 135°), permitiendo calcular los parámetros de Stokes I, Q y U, así como el grado y ángulo de polarización lineal de la fuente observada en una sola exposición. En este artículo presentamos el diseño de un módulo WeDoWo en SiO_2 (Sílice Cristalina) y describimos la caracterización realizada en laboratorio a distintas longitudes de onda y su posterior calibración. De igual manera mostramos la aplicación de este módulo para polarimetria astronómica utilizando el telescopio de 1 metro del Observatorio Astronómico Nacional de Tonantzintla, Puebla (OAN-TNT), exponiendo las ventajas y limitaciones que presenta esta técnica y el rendimiento óptimo que se puede lograr.

ABSTRACT

The Wedge Double Wollaston (WeDoWo) or "double Wollaston" module is a device capable of displaying four images of a single field of view (FOV); each image corresponds to a different polarization angle (0°, 45°, 90°, and 135°), providing enough information for the Stokes I, Q, and U parameters calculus and the linear polarization angle and fraction values retrieved from the source observed, in this case, an astronomical source, in a single exposure (single-shot). In this paper, we present the design of a SiO2 (Crystalline Silica) WeDoWo module, describing the characterization process carried out in the laboratory and the subsequent calibration. Likewise, we show the application of this module for imaging astronomical polarimetry using the 1.0-meter telescope of the National Astronomical Observatory from Tonantzintla, Puebla (OAN-TNT), illustrating the advantages and limitations of this technique and the optimal performance of this module.

Key Words: Polarization — instrumentation: polarimeters: WeDoWo — methods: observational — techniques: polarimetric

1. INTRODUCTION

Polarization at visible and near-infrared (NIR) wavelengths gives us fundamental information about the scattering of light produced by various physical

[1]Instituto Nacional de Astrofísica, Óptica y Electrónica. Luis Enrique Erro #1, Sta. María Tonanzintla, 72840, San Andrés Cholula, Pue.

[2]Tyndall National Institute. Lee Maltings Complex Dyke Parade, Cork, Cork, T12 R5CP, Ireland.

phenomena that occur in astronomical objects; one of them is the interaction of the light with the circumstellar medium (CSM) that surrounds the stars, produced during their evolution. Polarimetric measurements allow us to understand light interaction with the CSM better, identify the point of origin of the light, and constrain other parameters of the dust distribution. In some instances, the polarization angle is related to a magnetic field, where the longer axis of dust particles acquires preferential orientation, with the media acting as a dichroic. Polarimetric phenomena can occur in reflection nebulae, star-forming regions, (Tinbergen 1996; Clarke 2009), supernova remnants (Ritacco 2016), stars and planetary nebulae (Scarrott & Scarrott 1994; Gledhill et al. 2001; Serrano-Bernal et al. 2020; Devaraj et al. 2018), and it can be caused by dichroic extinction from dust grains which position is associated to local magnetic fields (Hiltner 1949; Lazarian & Hoang 2007), by the presence of synchrotron radiation or by the thermal emission of the dust (Ritacco 2016; Tinbergen 1996; Clarke 2009).

Nowadays, there are several instruments capable of measuring image polarization of astronomical objects and phenomena at different wavelengths. Some designs contain mechanical elements such as a rotating half-wave plate (HWP), a useful component for wide-field observations. Examples of this kind of instrument are POLICAN, SIRPOL, and MIMIR in the NIR band or NIKA in the submillimeter waveband (Devaraj et al. 2018; Ritacco 2016). However, because of the long exposures needed, the HWP may introduce instabilities in the system or be sensitive to the change in the sky quality. A solution is to remove the rotating component using a birefringent material capable of splitting the light into its ordinary and extraordinary components, which allows recovery of the polarization of the light. One proposed solution to the rotation problem was the Wollaston prism, which splits the light into two orthogonal components but requires an HWP to fully measure the entire linear polarization. Oliva (1996) proposed a new design using a double Wollaston. Each one gives the ordinary and extraordinary components of the incident light: paired in 0° and 90° angles for the first Wollaston, 45° and 135° for the second. It contains an entrance "Wedge," which helps split the FOV and redirect it to each Wollaston. This design is called the "Wedge Double Wollaston´´ (WeDoWo). Figure 1 shows the design developed by Oliva (1996). This device is already implemented in some polarimeters (Helhel et al. 2022; Pernechele et al. 2015), and they are focused on performing observations of small astronomical sources (i.e., small solar system bodies or stars). The principal difference concerning polarimeters using a rotating optical element is that the WeDoWo class of polarimeters can retrieve enough information to make a polarization analysis of the observed FOV within a single exposure, which represents an advantage in reducing the noise and the uncertainties caused by the mechanical and optical components.

In this paper, we present the design of the WeDoWo module and its application to imaging astronomical polarimetry. We perform simulations using specialized software for optical design (Ansys®Zemax OpticStudio) and per-

form tests in the laboratory and on a 1.0-meter telescope. In sections 2 and 3, we present the current design of the WeDoWo module, the considerations that must be taken into account to perform the laboratory tests, and the results of the characterization and calibration. In section 4, we show the performance of the WeDoWo on astronomical observations focusing on the polarimetric standard stars and extended sources like Frosty-Leo, a pre-planetary nebulae with an angular size $\leq 1'$. Finally, the conclusions of this work are presented in section 5.

2. THE WEDOWO MODULE

As described in section 1 and illustrated in figure 1, the WeDoWo module is designed to display simultaneously four images of the same FOV, allowing to compute the Stokes Q and U parameters related to the linear polarization fraction and angle. Section 2.1 describes the Stokes parameters more profoundly.

In this case, the WeDoWo module was initially designed for the 2.1-meter telescope of the Guillermo Haro Astrophysical Observatory (OAGH) by Medina (2020) for a one-shot polarimeter specialized for observing minor bodies in the Solar System. Designed and manufactured on SiO_2 following the Oliva (1996) considerations, the lack of chromatic difference between two or more elements and the relatively high Abbe number ($V_d = 70.132$ for the crystalline silica) make that the performance of the WeDoWo, described in figure 1 can be achieved. The Wedges and the Wollaston have an angle of $\alpha = \pm 3.2°$, and $\beta = \pm 60°$, respectively. Figure 2 shows the simulation performed in OpticStudio for a collimated wavefront and an ideal convergent lens at the module's output to show the ideal performance and field distribution; further description of this design is reported by Medina (2020). It's important to consider the different configurations of the Wedges and the Wollaston surfaces related to the values of α and β to model the WeDoWo performance correctly. Figure 3 shows the WeDoWo module, built by Bernhard Halle Nachft. Section 3 describes the different tests performed once the module was in INAOE's laboratory.

2.1. *Stokes Parameters and Polarization of the WeDoWo Module*

2.1.1. *Stokes Parameters and Polarization*

The Stokes parameters are quantities that describe the polarization fraction and angle of the incident light. For an instrument with a WeDoWo module as a main polarimetric device, the Stokes parameters expressions for the linear polarized incident light are enunciated in eq. 1 (Helhel et al. 2022; Tinbergen 1996; Shurcliff 1962):

$$\begin{aligned} I &= I_{0°} + I_{90°} \quad or \quad I_{45°} + I_{135°}. \\ Q &= I_{0°} - I_{90°}. \\ U &= I_{45°} - I_{135°}. \end{aligned} \tag{1}$$

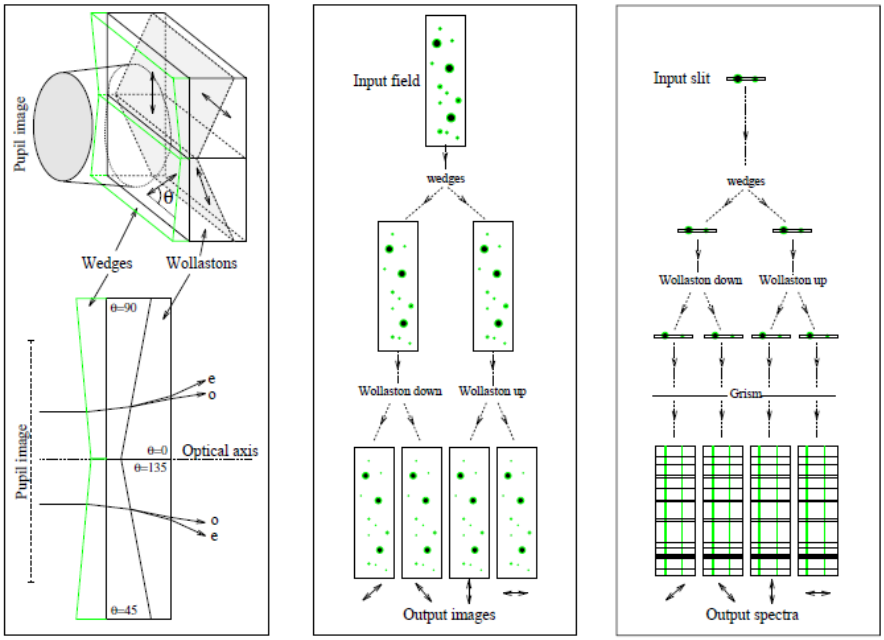

Fig. 1. *Left*: Schematic representation of the WeDoWo module and its behavior. To prevent the field's cross-talk, the Wedge's angles are calculated to split the field in four. *Center*: Illustration of how the system makes four polarized images of a stellar field. *Right*: Illustration of how the system with an additional disperse component can make four polarized spectra of two stars (Oliva 1996).

The analysis of the Stokes I parameter can come out separately for each Wollaston, i.e., $I_{W1} = I_{0^\circ} + I_{90^\circ}$, and $I_{W2} = I_{45^\circ} + I_{135^\circ}$, which allows a precise analysis of the polarization fraction by normalizing the Stokes parameters $q = Q/I_{W1}$ and $u = U/I_{W2}$. The linear polarization fraction and angle can be obtained with the following eq. 2 and 3:

$$P = 100\sqrt{q^2 + u^2}. \tag{2}$$

$$A = \frac{1}{2}\, arctan\left(\frac{u}{q}\right). \tag{3}$$

These relations allow us to determine the fraction and angle of linear polarization, regardless of whether the light comes from an astronomical object or a controlled source in the laboratory.

2.1.2. *Linear polarization debiasing*

The measurement corresponding to the different polarization angles carry some statistical uncertainties, and error propagation can be carried out with standard techniques (Bevington & Robinson 2010; Serrano-Bernal 2021):

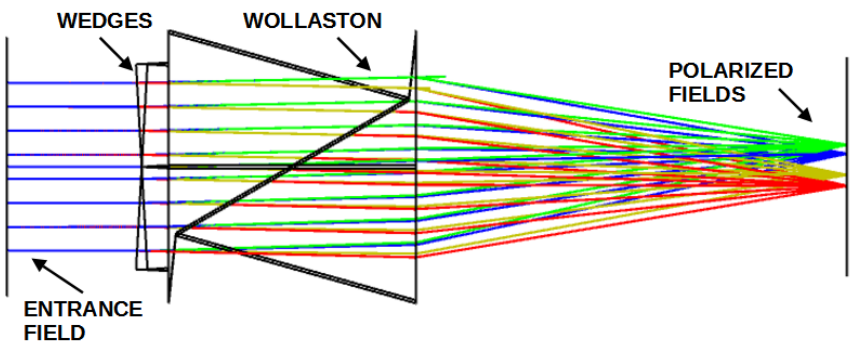

Fig. 2. Final optical design of the WeDoWo module implemented in Zemax *OpticStudio*. Each color represents a polarized field. Green: Vertical polarization, blue: horizontal polarization, yellow: 45° polarization, red: 135° polarization. This schematic is only for illustrative purposes, and the structure of the built WeDoWo is shown in Figure 3.

$$\sigma_x^2 = \sigma_u^2 \left(\frac{\partial x}{\partial u}\right)^2 + \sigma_v^2 \left(\frac{\partial x}{\partial v}\right)^2 + \sigma_w^2 \left(\frac{\partial x}{\partial w}\right)^2. \tag{4}$$

Equation 4 considers the contribution of error for a parameter X depending on the variables u, v and w, i.e., $X = f(u, v, w)$. The nature of the uncertainties depends on the measurement instrument. In the case of imaging astronomy, the most common devices are the Charge-Couple Devices (CCDs). The corresponding uncertainties are related to the readout noise and the system gain (Howell 2006) and can be described with the equation 5 as follows:

$$\sigma_{ADU} = \sqrt{\frac{F}{G}}. \tag{5}$$

The Analog Digital Units (ADUs) are the analog readout from the CCD transformed into digital units. F is the value of each pixel of the detection matrix, and G is the gain of the CCD's system. The statistical uncertainties of each field and polarization angle are represented as $\sigma_{0^\circ}, \sigma_{45^\circ}, \sigma_{90^\circ}$, and σ_{135°. The propagation through the Stokes I, Q, and U parameters can be calculated with the enunciated in the equations 6, 7 and 8 as follows:

$$\sigma_I = \sqrt{\sigma_{0^\circ}^2 + \sigma_{90^\circ}^2} \quad or \quad \sqrt{\sigma_{45^\circ}^2 + \sigma_{135^\circ}^2}. \tag{6}$$

$$\sigma_q = \frac{2}{I^2}\sqrt{\sigma_{0^\circ}^2 I_{90^\circ}^2 + \sigma_{90^\circ}^2 I_{0^\circ}^2}. \tag{7}$$

$$\sigma_u = \frac{2}{I^2}\sqrt{\sigma_{45^\circ}^2 I_{135^\circ}^2 + \sigma_{135^\circ}^2 I_{45^\circ}^2}. \tag{8}$$

σ_q and σ_u are the error propagation related to the Q and U normalized Stokes parameters. Statistical errors of $P(\sigma_P)$ and $A(\sigma_A)$ are related to the

Fig. 3. Final assembly of the WeDoWo module. This takes account the considerations exposed in Section 2 and its behaviour is the exposed in Figure 2.

error propagation of the Stokes elements under the relations described in the equations 9 and 10 as follows:

$$\sigma_P = \frac{100^2}{P}\sqrt{q^2 \times \sigma_q^2 + u^2 \times \sigma_u^2}. \tag{9}$$

$$\sigma_A = \frac{100^2}{2P^2}\sqrt{u^2 \times \sigma_q^2 + q^2 \times \sigma_u^2}. \tag{10}$$

The error propagation of the Stokes parameters is contained in the quadratic sum related to the polarization fraction expression (eq. 2); the statistical error makes a positive contribution to the measurement of polarization, introducing a bias value that's necessary to subtract. Equation 11 is the expression of the polarization difference between the average of the observed $\langle P \rangle$ and the real polarization fraction P_0.

$$\Delta P = \langle P \rangle - P_0. \tag{11}$$

The debiasing of the polarization fraction is performed by the *Ricean* correction, described in the eq. 12:

$$P_0 = \sqrt{P^2 - \sigma_P^2}. \tag{12}$$

Bias correction is necessary even for the case of high signal-to-noise ratio (SNR) values where the polarization values are small and σ_P and ΔP are similar (Patat & Romaniello 2004). The eq. 7 and 8 represent a threshold value in the future polarimetric data analysis to keep the relevant information of the observed source in an imaging analysis.

2.2. *A non-ideal Wollaston prism: effects and considerations*

2.2.1. *Parameter-t*

The WeDoWo module comprises two Wollaston prisms with a different linear polarization angle orientation. In an ideal case, the Wollaston prism splits incoming unpolarized light into identical fractions, i.e., intensity in ordinary and extraordinary axis are equal to $I/2$ where I represents the total intensity of the incident light (Helhel et al. 2022; Patat & Romaniello 2004). But in the case of nonideal Wollaston prims, we need to introduce the parameter-t or the transmission parameter (Helhel et al. 2022; Patat & Romaniello 2004). The equation 13 gives the intensity of each polarized field.

$$\begin{aligned} I_0 &= t_1 I. \\ I_{90} &= (1 - t_1) I. \\ I_{45} &= t_2 I. \\ I_{135} &= (1 - t_2) I. \end{aligned} \tag{13}$$

Where t_1 and t_2 are the parameters-t of each Wollaston and, in an ideal scenario, both are equal to 1/2 (Helhel et al. 2022; Patat & Romaniello 2004). If we derive the equation 13, we can replace the total intensity with the real intensity of each field. Equation 14 represents the real fluxes of each polarized field:

$$\begin{aligned} I'_0 &= I_0/(2t_1). \\ I'_{90} &= I_{90}/(2(1 - t_1). \\ I'_{45} &= I_{45}/(2t_2). \\ I'_{135} &= I_{135}/(2(1 - t_2)). \end{aligned} \tag{14}$$

The importance resides in the fact that once we know the real values of the parameter-t of each Wollaston, it is possible to correct the fluxes of each field and make the first polarimetric correction (Helhel et al. 2022; Patat & Romaniello 2004).

2.2.2. *Instrumental polarization*

Any optical system could introduce some instrumental polarization values related to its configuration, so it is necessary to consider this to recover the actual incident polarization degree. The description of instrumental polarization can be performed by the Mueller matrix represented by the equation 15 as follows:

$$\mathbf{M_i}(x, y) = \frac{1}{(1 + p)} \begin{bmatrix} 1 & p\cos 2\theta & p\sin 2\theta \\ p\cos 2\theta & 1 - p\sin^2 2\theta & ps\cos 2\theta \\ p\sin 2\theta & p\sin 2\theta\cos 2\theta & 1 - p\cos^2 2\theta \end{bmatrix}. \tag{15}$$

The matrix of equation 15 corresponds to an ideal Mueller matrix of polarization, where $p = p(x, y)$ and $\theta = \theta(x, y)$ are the instrumental polarization

fraction and angle across the FOV, making it possible to estimate the instrumental Stokes parameters Q_i and U_i which can be represented by the system described in equation 16 as follows:

$$\begin{aligned} I_i(1+p) &= I_0 + Q_0 p\cos 2\theta + U_0 p\sin 2\theta. \\ Q_i(1+p) &= I_0 p\cos 2\theta + Q_0(1 - p\sin^2 2\theta) + U_0 p\sin 2\theta\cos 2\theta. \\ U_i(1+p) &= I_0 p\sin 2\theta + Q_0 p\sin 2\theta\cos 2\theta + U_0(1 - p\cos^2 2\theta). \end{aligned} \tag{16}$$

where I_0,Q_0, and U_0 are the incident Stokes parameters. For an unpolarized source, the equation 16 is simplified, and $p(x, y)$ and $theta(x, y)$ can be derived immediately. The problem becomes more complicated with an incoming polarized light beam. Still, in this case, the system can be simplified assuming that $p \ll 1(100\%)$ and $P \ll 1(100\%)$ since instrumental polarization is typically less than a few percent (Patat & Romaniello 2004), equation 16 can be rewritten as follows:

$$\begin{aligned} I_i &\simeq I_0. \\ Q_i &\simeq Q_0 + I_0 p\cos 2\theta. \\ U_i &\simeq U_0 + I_0 p\sin 2\theta. \end{aligned} \tag{17}$$

Equation 17 represents a set of approximate expressions useful to evaluate the instrumental polarization, provided that the input polarization is known and the observed source covers a large fraction of the FOV. Solving equation 17 for $p(x, y)$ and $\theta(x, y)$ yields:

$$p_1 \simeq \frac{Q_i - Q_0}{I_0\cos 2\theta}. \tag{18}$$

$$p_2 \simeq \frac{U_i - U_0}{I_0\sin 2\theta}. \tag{19}$$

$$\theta \simeq \frac{1}{2}\arctan\frac{U_i - U_0}{Q_i - Q_0}. \tag{20}$$

Where p_1 and p_2 are two independent estimates of $p(x, y)$ and can be averaged to increase the accuracy due to the non-polarized nature of the source and the value of the instrumental polarized related to the optical system (Patat & Romaniello 2004).

2.2.3. *The transmittance ratio R*

Due to the possible difference of transmission between the two Wollaston that composes the module, it is possible to introduce the transmittance ratio (R) value, represented by the ratio of the two intensity expressions of the equation 1 as follows:

$$R = \frac{I_{45} + I_{135}}{I_0 + I_{90}}. \tag{21}$$

The transmittance ratio could be applied to the instrumental Stokes parameters correction as follows Helhel et al. (2022):

$$\begin{bmatrix} I \\ Q \\ U \end{bmatrix} = \begin{bmatrix} I_i \\ R \times Q_i \\ U_i \end{bmatrix}. \tag{22}$$

The application of the transmittance ratio requires, for the computation of the polarization fraction, the implementation of the second intensity expression of the equation 1 (i.e., $\mathrm{I} = I_{45} + I_{135}$) considering the respective error propagation.

2.3. *Final description of the WeDoWo module*

Taking into account the considerations enumerated in the previous sections, a WeDoWo-based instrument can be cataloged like a four-intensity polarimeter, i.e., the four intensities can be measured simultaneously (Compain et al. 1999), and can be described by the following expression:

$$\begin{bmatrix} I_1 \\ I_2 \\ I_3 \\ I_4 \end{bmatrix} = \mathbf{AS}. \tag{23}$$

Where $\mathbf{A}$ is the characteristic matrix of the polarimeter, and $\mathbf{S}$ is the input Stokes vector. The WeDoWo module can only work with linear polarized incident emission, so in this case, the structure of the equation 23 is represented by:

$$\begin{bmatrix} I_1 \\ I_2 \\ I_3 \\ I_4 \end{bmatrix} = \begin{bmatrix} t_1 & t_1 \cos 2\theta_{o_1} & t_1 \sin 2\theta_{o_1} \\ t_{11} & t_{11} \cos 2\theta_{e_1} & t_{11} \sin 2\theta_{e_1} \\ t_2 & t_2 \cos 2\theta_{o_2} & t_2 \sin 2\theta_{o_2} \\ t_{21} & t_{21} \cos 2\theta_{e_2} & t_{21} \sin 2\theta_{e_2} \end{bmatrix} \begin{bmatrix} I_{in} \\ Q_{in} \\ U_{in} \end{bmatrix}. \tag{24}$$

Where θ_{o_1}, θ_{o_2}, θ_{e_1} and θ_{e_2} are the orientation angles for the ordinary and extraordinary transmission axis for the first and the second Wollaston respectively. t_1, t_{11}, t_2 and t_{21} are the parameter-t values, described previously in subsection 2.2.1, for the first and second Wollaston of the module, where $t_{11} = (1 - t_1)$ and $t_{21} = (1 - t_2)$. If $\theta_{o_1} = 0°$, $\theta_{e_1} = 90°$, $\theta_{o_2} = 45°$ and $\theta_{e_2} = 135°$, the expressions from equation 1 can be easily derived taking account the following:

$$\mathbf{S} = \mathbf{A}^{-1}[I_1, I_2, I_3, I_4]^T \tag{25}$$

Equation 24 is a variation of the polarimeter characteristic matrix exposed by Compain et al. (1999), with the main change in the matrix size due to the lack of capability to detect circularly polarized incident emission. Also, the

representation changes; in this case, we consider the orientation angles related to the ordinary and extraordinary transmission axis instead of the ellipsometric angles exposed by Compain et al. (1999). However, both representations are equivalent, and the equation 24 can be represented with the ellipsometric angles, with their respective considerations.

3. LABORATORY CHARACTERIZATION

The previous modeling and simulation made in OpticStudio, shown in figure 2, demonstrates that the performance of the designed WeDoWo module can satisfy the requirements for which it was intended. The laboratory test aims to prove the reliability of the simulations and find the actual characteristics of a non-ideal WeDoWo module in terms of the location of the polarized fields, which describes the configuration of each Wollaston, and the response of the module to an incident polarized light beam. In the following, we describe the characterization process in the laboratory and the results of these experiments.

3.1. *Characterization process*

For a successful characterization process, plenty of considerations must be taken about the position of the different optical elements. First of all, it is necessary to align the optical components properly. Figure 4 shows a schematic representation of the proper alignment of the elements of the WeDoWo module. Figures 5 and 6 show the implementation of the previous schematic diagram. Second, the entrance pupil must be controlled to avoid the crosstalk between polarized intensities, constraining the efective FOV. In the following, we enumerate the optical components involved in this characterization process:

1. Optical tables and support elements and tools for the WeDoWo and the optical elements. For this purpose, a special mount was developed for the WeDoWo, which consists of a couple of CPVCs of 1 inch in diameter ($2.56cm$).

2. Newport 20LP-VIS-B linear analyzer installed on a Newport RSP-2T rotational coupler. This element is necessary to find the position of each field.

3. Biconvex optic lens with a focal distance of $f = 13.62cm$. Useful for the focus of the polarized fields.

4. "SBIG STF-8300" Optical CCD with a detection matrix of 3352×2532 pixels and a saturation level of 65536 ADUs, with its respective CCD RGB filters.

5. Newport Fabry-Perot laser module $\lambda = 635nm$

6. Blank field positioned and illuminated by reflection to generate the low-polarized light source.

For the low-polarized source emission, we use an emission light diode (LED) and a blank field, causing the reflection of the LED's light to the optical system. Saito et al. (2022) enunciates that LED devices have the characteristic of emitting low-polarized light related to the material that surrounds the chip (the epoxy resin) and the orientation of the LED's emission to the optical system. Still, in the case of emission coming from the top of the LED's structure, the polarization fraction is minimum but not zero, i.e., $0-9\%$. The low-polarized source will aid us in constraining the location of the fields and performing an initial polarimetric analysis to show the capabilities of the WeDoWo module to produce quality polarimetric data.

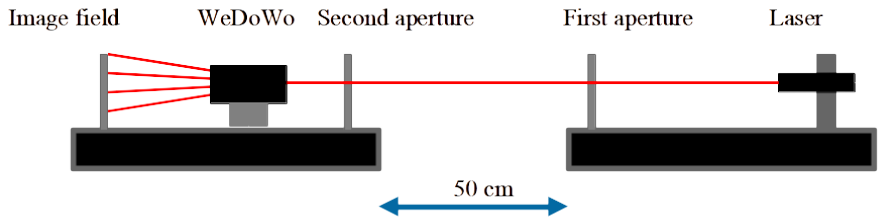

Fig. 4. Schematic representation of the alignment process of the optical system on the test-bench

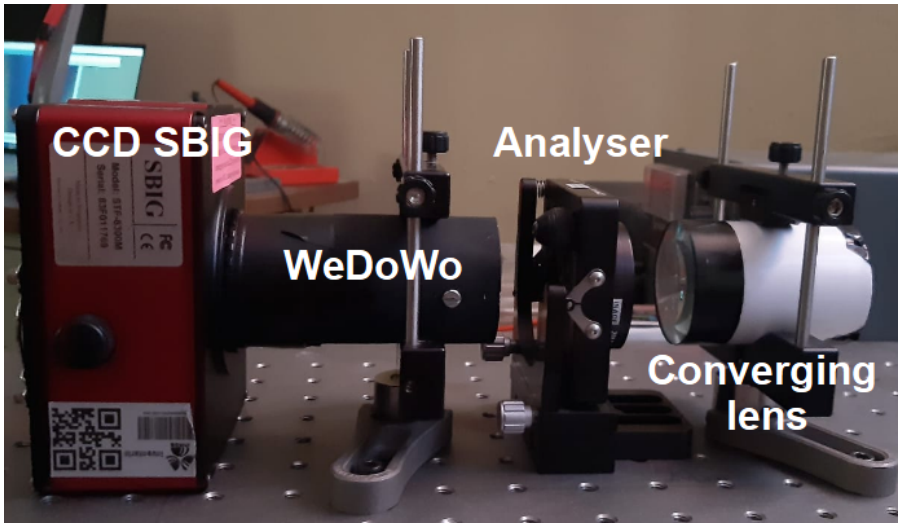

Fig. 5. Final distribution of the test-bench with the Newport analyser

Once the alignment of the optical components is performed and the entrance field is appropriately controlled, we need to make a location for each

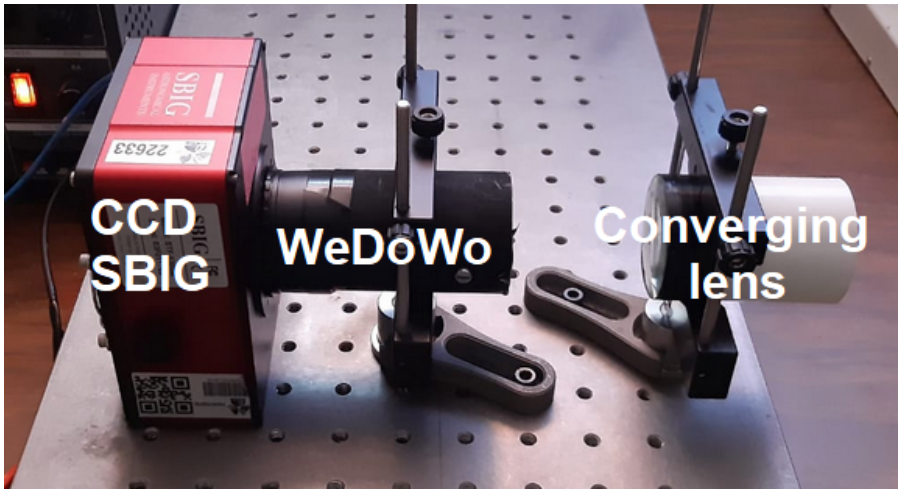

Fig. 6. Final distribution of the test-bench without the analyser

field to find its transmission axis orientation angle. In this instance, a linear analyzer device is crucial; the task is to match the polarizer's transmission axis with the different transmission axes that compose the module. Theoretically, the transmission axes angle distribution is $\theta_{o_1} = 0°$, $\theta_{e_1} = 90°$, $\theta_{o_2} = 45°$ and $\theta_{e_2} = 135°$ for the first and second Wollaston respectively, but is necessary to locate the position of the fields before any polarimetric analysis. Figure 5 shows the position of the analyzer in the system, and Figure 7 shows the results of these tests, showing that the $\theta_{o_1} = 0°$, $\theta_{e_1} = 90°$ corresponds to the bottom location of the image, and $\theta_{o_2} = 45°$ and $\theta_{e_2} = 135°$ corresponds to the top.

With the proper location of the fields, the analyzer is retired from the optical system. Then, we perform several data acquisition of the FOV for the polarimetric analysis. We trim each polarized field from the observed data, as shown in figure 8, and analyze it following the equation 1 expressions.

The maps corresponding to the normalized Stokes Q and U parameters are shown in figure 9 with their respective histogram that shows the value distribution across the observed FOV (Figure 10). The calculation of the polarization fraction and angle is performed with equations 2 and 3, respectively. Figures 11 and 12 show the spatial distribution and the value distribution of the polarized fraction obtained from the blank-field observations. The average values for the normalized Stokes parameters Q and U are $\langle q \rangle = 0.060 \pm 0.022$ and $\langle u \rangle = 0.024 \pm 0.020$, and the average polarization fraction and angle values are $\langle P \rangle = 6.8\% \pm 2.35\%$ and $\langle A \rangle = 79.5° \pm 9.558°$, retrieved from the observational data, with the sigma values containing the product of the error propagation compute and the statistical uncertainties analysis within the polarization fraction and angle values. The values reported for the blank-field observations remember the values reported by Saito et al. (2022) about the polarization fraction value for an LED, aided with a reflection surface that in-

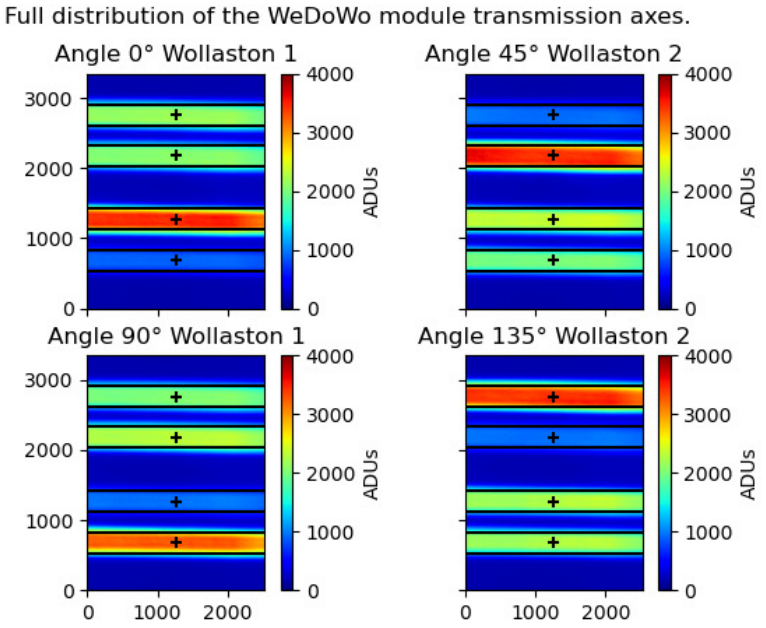

Fig. 7. Four polarized fields plotted each one by a position of the linear analyzer, matching the transmission axis of each Wollaston. Black frames highlight the fields, and the field corresponding to the analyzer's transmission angle shows the maximum value of the color bar reported for each image.

troduces an extra polarization fraction value for our measurement. With these results, we can conclude that the WeDoWo module can display four fields of the observed FOV with enough information for the calculus of the Stokes parameters of the linear polarization emission and the polarization fraction and angle values. As aforementioned in section 2.2.2, the values related to the instrumental polarization are a few percentages (i.e., $\langle P_{inst} \rangle \ll 100\%$) and, for the configuration of the optical system, the only element that can introduce instrumental polarization values are the biconvex optic lens.

To conclude, the laboratory tests helped find the characteristics of the double Wollaston module in terms of the transmission axis of each Wollaston and their angle orientation, the location of the fields related to each transmission axis, and finally, calibrating how the polarimetric data from the WeDoWo observations must be computed for obtaining satisfactory processed data.

4. APPLICATION IN ASTRONOMICAL OBSERVATIONS

Once the laboratory tests have been performed, the next step is to prove the capabilities of the WeDoWo module in making astronomical polarimetric observations. For this, an experimental instrument was implemented in the 1.0-meter telescope of the National Astronomical Observatory of Tonantzintla,

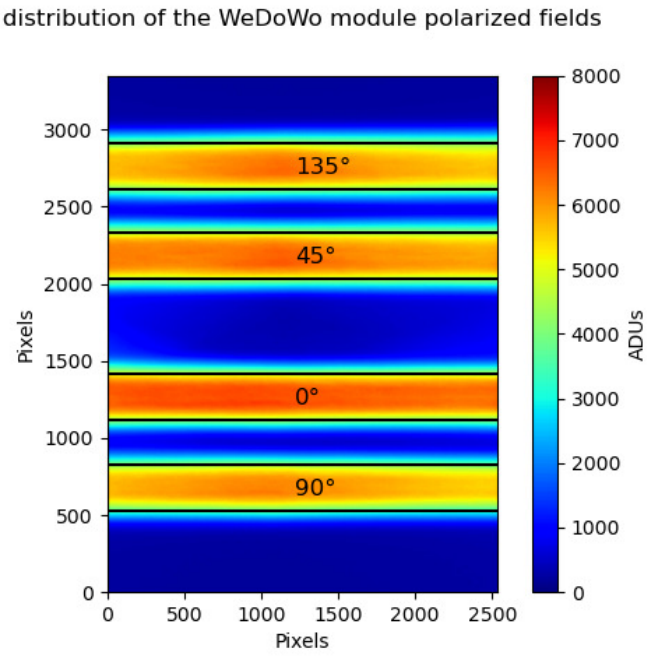

Fig. 8. Distribution of each polarized field for a flat blank field in the detector.

Puebla (OAN-TNT), which is an instrument with optical characteristics that allow one split of the fields on its detection matrix, which means it is possible to recover information on the astronomical sources observed and carry on polarimetric analyses of them via one-shot observations.

4.1. *Telescope Overview*

The OAN-TNT 1.0 meter telescope is Cassegrain type with an equatorial mount and an effective focal distance of $f_{eff} = 15240$ mm, meaning that it is an $f/15$ telescope and has a plate scale of $PS = 13.53$ arcsecs/mm. The "CCD STL-1001E (SBIG)", the optical detector of the telescope, has a detection matrix of 1024×1024 pixels with a pixel size of 24×24 μm^2. The plate scale of this system is 0.325 arcsecs/pixel, and the total recovered field is 5.5×5.5 $arcmin^2$. This CCD detector incorporates a Johnson filter wheel, which is essential for polarimetric observations at different wavelengths. Table 1 shows the various characteristics of the Jonhson filters.

Since the WeDoWo polarimeter is mounted on a telescope that doesn't match its original design parameters and has no correction lenses as reported by Medina (2020), small optical aberrations might affect our images. However, we did not notice any evidence of such aberrations in our results. Therefore, we conclude that the WeDoWo module is useful for studying the polarization of point sources and small extended objects.

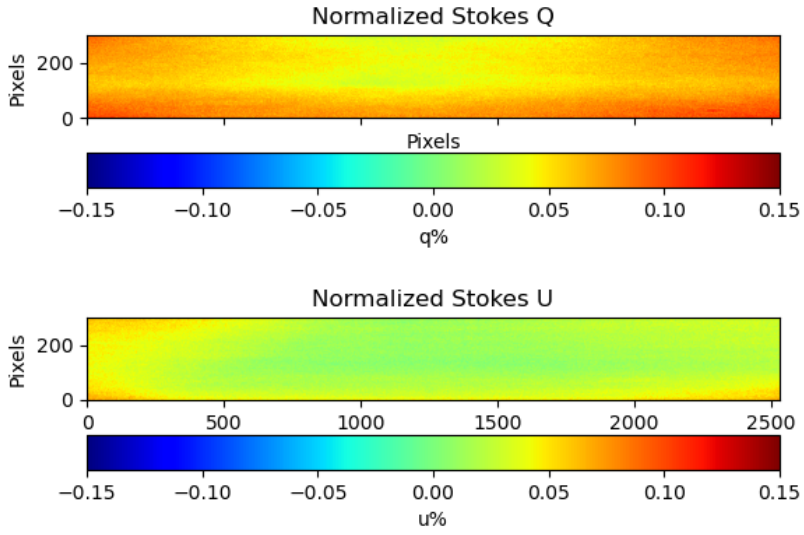

Fig. 9. *Top:* Normalized Q Stokes and, *Bottom:* Normalized U Stokes imaging fields, obtained by the trim and calculation of the blank field observation shown in figure 8 using the eq. 1 described in section 2.

4.2. *Experimental Polarimeter*

Several simulations were performed to find the best implementation of the WeDoWo module in the telescope. In this case, without any other corrective lenses, the WeDoWo module must be positioned at a distance of $200mm$ from the CCD detector to obtain a satisfactory split and distance between the fields and avoid cross-talk between them, figure 13 shows a schematic of the distribution on the CCD detector of the four fields and also shows the analysis performed to get the optimal position of the WeDoWo module. Figure 14 shows the physical design implemented for holding the WeDoWo module on the telescope. One of the primary considerations of the implementation (besides the four fields display) was the implementation that attached the CCD to the telescope with no changes to the original structure.

Figure 15 shows the installation of the holder in the telescope mechanism and the optical CCD of the OAN-TNT. To better display the four fields, the consideration was to rotate the WeDoWo 45° in a counter-clockwise direction, giving us a rotation of the transmission axes obtained in the four fields. Figure 16 describes graphically the critical features for the further polarimetric analysis of the target astrophysical sources.

Figure 17 shows the observations performed at the OAN-TNT corresponding to the schematic diagram of figure 16. The first stage of the implementation is successfully done; the observed FOV with the astrophysical source has

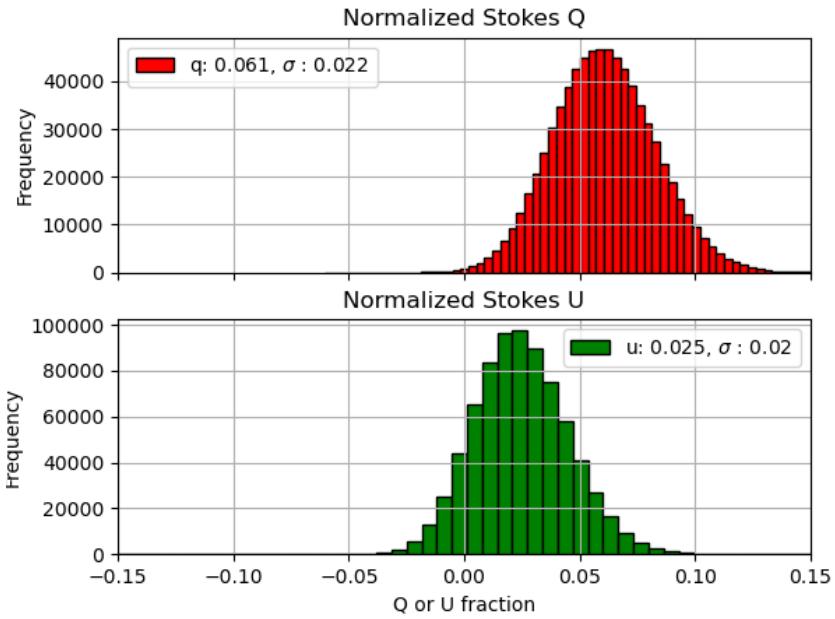

Fig. 10. *Top:* Normalized Q Stokes and, *Bottom:* Normalized U Stokes distribution values, obtained by the trim and calculation of the blank field observation shown in figure 8 using the eq. 1 described in section 2.

been divided into four fields, each corresponding to a different transmission axis orientation and, consequently, to a different polarization angle, allowing a polarimetric analysis using only a single exposure. The next stage is to test the system's performance and capability to recover the actual polarization fraction and angle. The laboratory tests, exposed in section 3, ensemble the path of the data reduction that must be performed for the observational astrophysical data.

4.3. *Calibration*

The first step of the calibration process is to observe a non-polarized standard star to find the approximate values of the parameter-t, exposed in section 2.2.1, instead of the intrinsic possible bias caused by the instrumental polarization; it's possible to make an initial correction of the parameter-t values of each Wollaston that could reveal the true value of the instrumental polarization. Once this correction is performed, the instrumental polarization and the polarization bias correction can be performed using the equation 12, showing the true value of the non-polarized sources, in this case, an average value of $\langle P \rangle \approx 0\%$. For the validation stage, we perform observations for polarimetric standard calibration sources, focusing on retrieving the reported

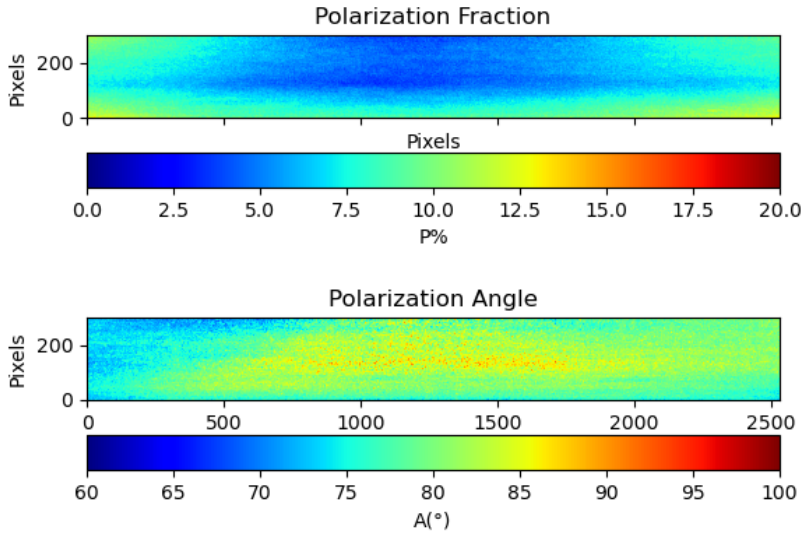

Fig. 11. *Top:* Polarization fraction and, *Bottom:* Polarization angle imaging fields, obtained by the trim and calculation of the blank field observation shown in figure 8 using the eq. 1 described in section 2.

value of polarization fraction and angle. Table 2 enumerates the observed polarimetric standard stars chosen for the instrument calibration and validation, two non-polarized standard stars (HD 109055 and HD 154892), and two polarized standard stars (HD 154445 and HD 161056). The star's polarimetric information is taken from the Poidvein (2023) database.

For data analysis, we perform the same strategy that is exposed in section 3, modifying the analysis tool to make it focused on trimming a section of the field where the astronomical object appears, making standard techniques of aperture photometry, i.e., the sum of the values within a circular aperture, minus the average value of an external annular ring section for the sky subtraction and the possible correction for effects of the background in the polarimetric calculus (Patat & Romaniello 2004; Tinbergen 1996). For an accurate polarimetric analysis, the aperture radius must be big enough to include all of the star emission; for testing that, we perform some growth curves to find an aperture value where the cumulative flux of the source reaches a stable value (O'Connor et al. 2020). Figure 20 shows this task, performed for the HD 101656 observations, where we found that the cumulative relative fluxes of the four fields get stable after an aperture radius of 10 arcseconds.

Table 3 enumerates the original parameter-t values and their effects on the Q and U-normalized Stokes parameters. After the calibration, table 4 shows that once the parameter-t values are corrected, the Q and U Stokes

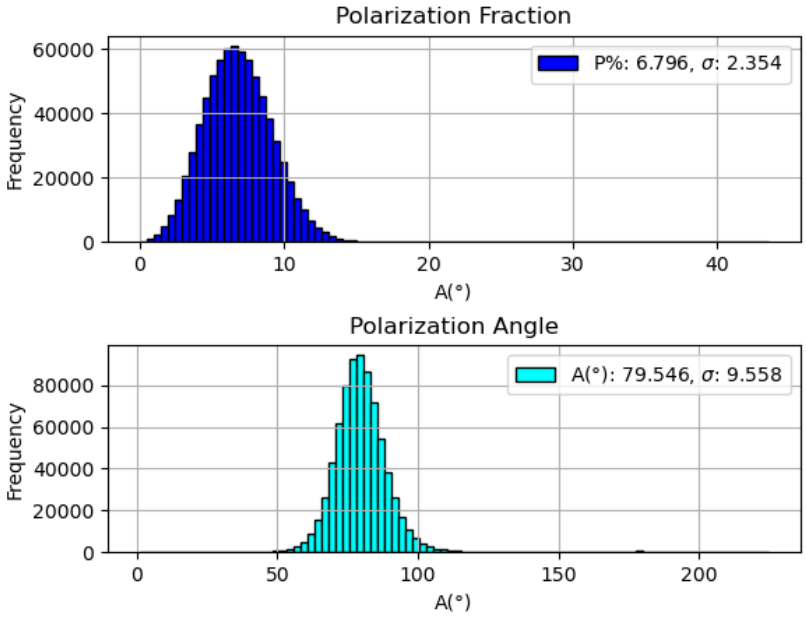

Fig. 12. *Top:* Polarization fraction and, *Bottom:* Polarization angle distribution values, obtained by the trim and calculation of the blank field observation shown in figure 8 using the eq. 1 described in section 2.

parameters have a value close to zero (or zero in some cases). Figures 18 and 19 complement the exposed in the tables with the distribution of the parameter-t values and the instrumental normalized Q and U Stokes values before and after the correction procedure. The values of the parameter-t and the Q and U Stokes parameters seem centered in zero and 0.5. Still, the uncertainty of the value causes an instrumental polarization value to reach the $\approx 1\%$.

After the calibration and correction procedure, with the same strategy, we perform the validation polarimetric analysis with the set of polarized standard stars. The comparison between the retrieved values with the reported values on the Poidvein (2023) database is enumerated in the table 5 and shows that the retrieved polarization fraction and angle values are close enough to the database values, validating the performance of the WeDoWo module for astronomical polarimetric observations in a single-shot technique.

4.4. *Observations*

To perform the observations, the astronomical sources must span a field of view of 1×1 $arcmin^2$ to avoid cross-talk between fields. This implies that our polarimeter is suitable for studying small objects, like stars (as shown

TABLE 1

LIST OF THE JOHNSON FILTERS SYSTEM

Filter	λ_c (Å)	FWHM $\Delta\lambda$ (Å)
U	3400	600
B	4200	1100
V	5400	1200
R	6000	700
I	8500	3000

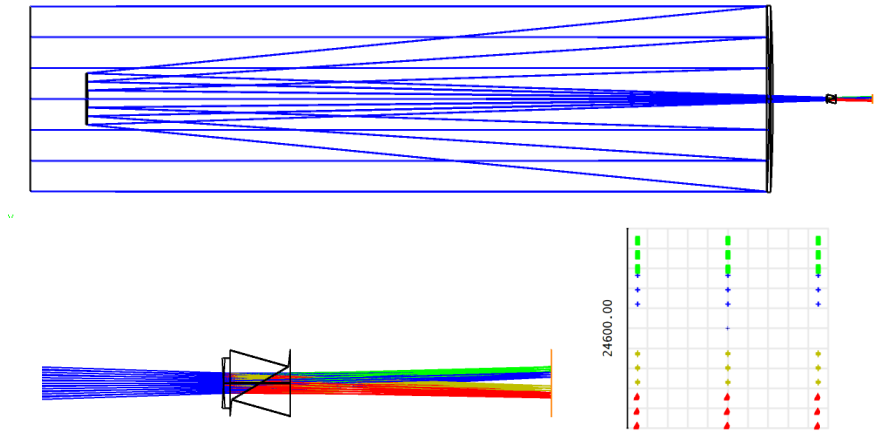

Fig. 13. *Top:* Simulation at the 1 meter OAN-TNT telescope of WeDoWo position. *Bottom left:* Zoom in from the top image, focusing on the weDoWo module's position that shows the splitting of the fields. *Bottom right:* Distribution of the polarized field over an area replicating the CCD detector's dimensions. The left number on the diagram is the CCD dimensions in μm. The color of the fields, as shown in figure 2, corresponds to a polarized field.

in the previous section to perform the calibration procedure on a telescope), asteroids, and compact extended objects, e.g., planetary nebulae.

We observed the Frosty Leo nebula (IRAS 09371+1212) in the full BVRI range to show WeDoWo's performance for extended emission astronomical objects. Exploring the observations, I-band data showed the best results in the way that the SNR of the nebular extended emission gets better recovered. The polarization fraction and angle are computed pixel by pixel for extended sources as described in Devaraj et al. (2018) and Serrano-Bernal et al. (2020). The results of these observations are shown in figure 21, where we also compare them against near-infrared polarization data from Serrano-Bernal et al. (2020).

As shown in figure 21, the polarization vectors in the nebula's central

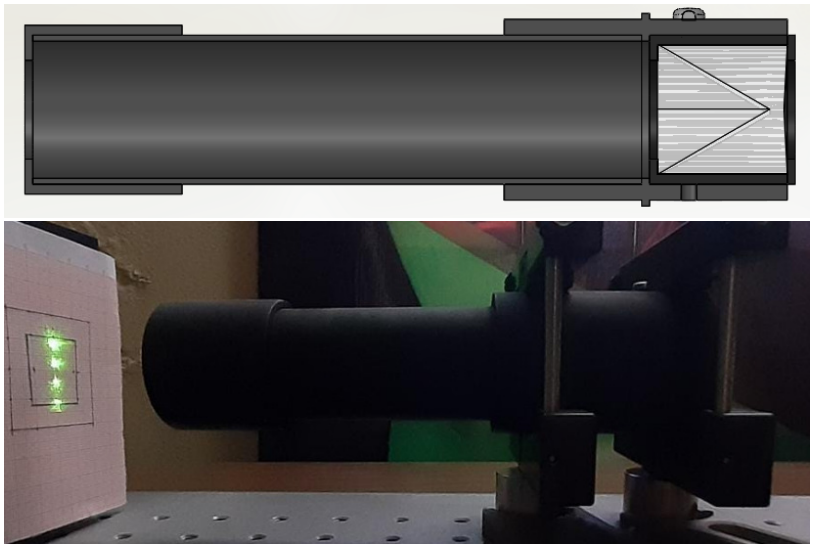

Fig. 14. *Top:* Transversal view of the WeDoWo module holder designed. *Bottom:* Implementation of the holder in the laboratory. The WeDoWo module lies inside.

TABLE 2

LIST OF THE SOURCES OBSERVED IN THE CALIBRATION STAGE.

Source	Kind	No. of observations
HD109055	Unpolarized	40 (10 Obs BVRI)
HD154892	Unpolarized	40 (10 Obs BVRI)
HD154445	Polarized	40 (10 Obs BVRI)
HD161056	Polarized	40 (10 Obs BVRI)

region show a centrosymmetric pattern in both optical (WeDoWo at I-band) and near-infrared (POLICAN at J-band Serrano-Bernal et al. (2020)). The centrosymmetric pattern of the polarization vectors is caused by the nature of the circumstellar medium, which is described as optically thin. The center of the pattern indicates the location of the primary emission source, and the scattered emission of the extended envelope is linearly polarized (Gledhill et al. 2001; Serrano-Bernal et al. 2020).

In Figures 22 and 23, we compare the results of the polarization analysis obtained from Frosty Leo's observations by POLICAN and the WeDoWo module. Figure 22 shows the polarization fraction maps, illustrating the extended structure distribution near the central system and in the north and south regions. In the case of WeDoWo's result, we can retrieve the extended structure distribution near the central system, where the centrosymmetric pattern lies. Compared with the POLICAN results reported by Serrano-Bernal et al. (2020), polarimetric observational results performed with the WeDoWo module denote the structure of the extended envelope product of the scattered

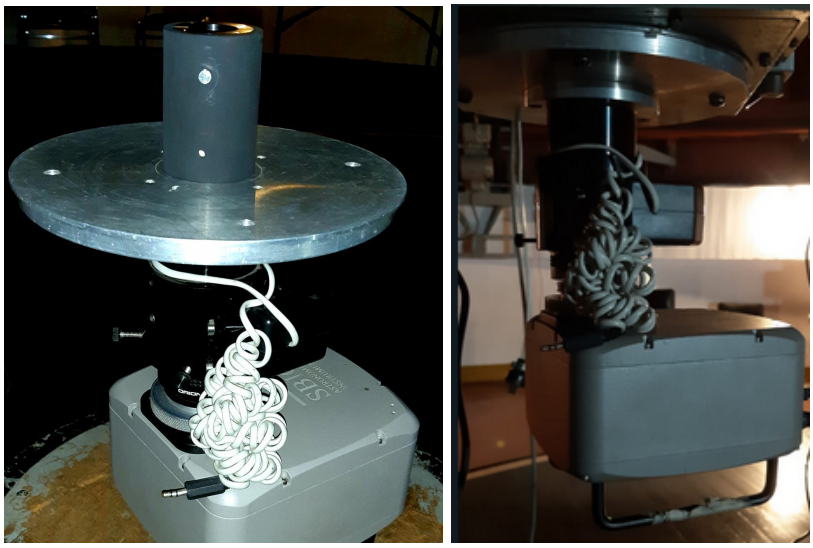

Fig. 15. *Left:* Mount of the WeDoWo holder inside the structure that attach the optical CCD to the telescope. The design takes into consideration this structure. *Right:* CCD structure properly attached to the telescope, the WeDoWo holder is already inside.

emission at the I-band. Figure 23 shows the similarities between polarization angle results for corresponding regions.

These results exposed in Figures 21, 22 and 23 also remember the distribution of the polarization fraction and angle reported by Scarrott & Scarrott (1994). However, it is necessary to perform more profound observations in the full BVRI to recover the polarization fraction and angle for the faint extended emission located to the north and south of the object, where the ansae structures reside and, according to Serrano-Bernal et al. (2020), the multiple scattering is the primary emission process in these regions, giving information about the extension of the dusty circumstellar medium that surrounds the system.

5. CONCLUSIONS

This paper presents the design of a WeDoWo module developed for the 2.1-meter telescope in OAGH for a one-shot polarimeter. We tested this module and described the steps and preliminary considerations needed to obtain the required parameters for full characterization and calibration. These procedures allow us to retrieve Stokes parameters of the linear polarization radiation and the observed sources' fraction and angle of polarization. The laboratory's description of the calibration helped us understand WeDoWo's behavior in a controlled environment. With this preliminary information, it is possible to plan better the calibration procedures that must be taken with the telescope. The 1.0-meter telescope of the OAN-TNT gives us an excellent chance

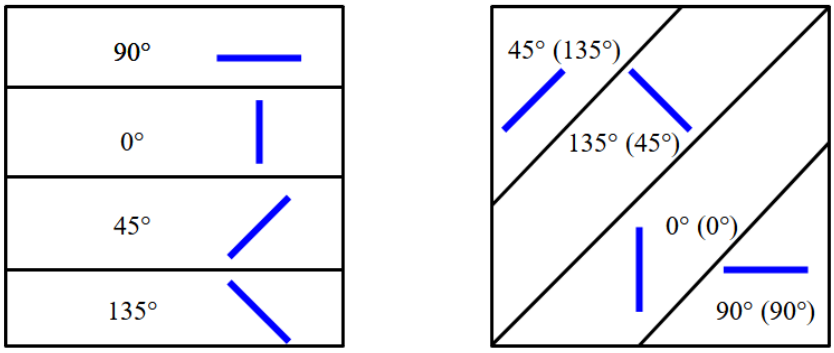

Fig. 16. *Left:* Original distribution of the polarized field. *Right:* 45° rotated WeDoWo distribution. The polarized fields change in function of the rotation. This consideration must be taken account to the polarization analysis of the observations.

TABLE 3

PARAMETER-T AND NORMALIZED Q AND U STOKES PARAMETERS MEAN VALUES WITH THEIR RESPECTIVE UNCERTAINTIES PER JOHNSON FILTER. RESULTS BEFORE THE CORRECTION PROCEDURE.

Johnson filter	t_1	$1-t_1$	t_2	$1-t_2$	q	σ_q	u	σ_u
I	0.515	0.485	0.495	0.505	-0.03	±0.001	-0.011	±0.011
R	0.512	0.488	0.501	0.499	-0.024	±0.001	0.001	±0.009
V	0.513	0.487	0.502	0.498	-0.026	±0.011	0.005	±0.007
B	0.525	0.475	0.497	0.503	-0.051	±0.004	-0.006	±0.006

to prove the WeDoWo capability to make astronomical observations. Despite the lack of an accurate optical system to correct the multiple optical aberrations that could be present, the results obtained via our observations prove that an instrument with these characteristics can perform polarimetric studies of astronomical sources. The only considerations that must be taken are that the observed sources must be small enough to avoid cross-talk between the polarized fields and use filters to reduce the possible chromatic aberration when using a birefringent material.

This work concludes that the WeDoWo module can perform astronomical polarimetric observations. The one-shot technique was satisfactorily implemented, producing the observatory's first polarimetric results. Frosty Leo's observations and results had the main objective of showing the capabilities of the WeDoWo module to retrieve the polarization fraction and angle values in extended sources with size $\leq$ 1 arcmin, which encourages us to continue the extended source investigations at the full BVRI bands of this kind of astronomical objects.

Fig. 17. *Left:* HD 109055, non polarized source. *Right:* HD 154445, polarized source. Both were observed with the 1.0-meter OAN-TNT telescope and the WeDoWo module.

TABLE 4

PARAMETER-T AND NORMALIZED Q AND U STOKES PARAMETERS MEAN VALUES WITH THEIR RESPECTIVE UNCERTAINTIES PER JOHNSON FILTER. RESULTS AFTER THE CORRECTION, PROCEDURE

Johnson filter	t_1	$1-t_1$	t_2	$1-t_2$	q	σ_q	u	σ_u
I	0.5	0.5	0.5	0.5	0.0	$\pm$0.001	0.0	$\pm$0.011
R	0.5	0.5	0.5	0.5	0.0	$\pm$0.001	0.0	$\pm$0.009
V	0.5	0.5	0.5	0.5	0.0	$\pm$0.011	0.0	$\pm$0.007
B	0.5	0.5	0.5	0.5	0.0	$\pm$0.004	0.0	$\pm$0.006

6. ACKNOWLEDGMENT

We express our special thanks to Claudio Pernechele for their advice about the design of the WeDoWo module and the polarimeter reported in Medina (2020). Also, we express special thanks to the National Astronomical Observatory of Tonantzintla (OAN-TNT) Puebla, Mexico, for support on the testing and observations in the 1.0-meter telescope and to the technical personnel of the Schmidt camera located on INAOE for the laboratory material provided for the characterization of the WeDoWo module. The authors thank CONAHCYT for supporting the following students: A. García-Pérez (CVU 1080875) and S. Medina (CVU 905889). E. O. Serrano-Bernal acknowledges CONAHCYT for the postdoc grant (CVU 480840) and support from the project CB-2016-01-281948. We also would like to thank the support for the following projects: 301917 "Actualización de la infraestructura cientifica del Observatorio astrofísico Guillermo Haro" and A1-S-54450 "Campos magnéticos en el medio interstellar." Finally, we thank INAOE for using the licenses associated

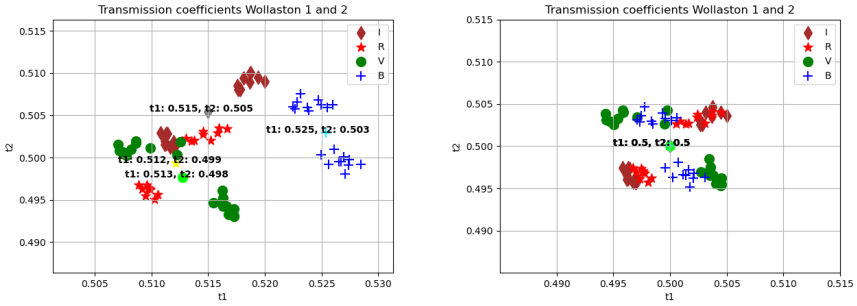

Fig. 18. *Left:* Plot of parameter-t of each Wollaston without the calibration procedure. *Right:* Plot of parameter-t of each Wollaston, calibration procedure implemented. In both cases, the colors represent the measurements in the Johnson filter system. The values in bold font represent the average values of the measurements.

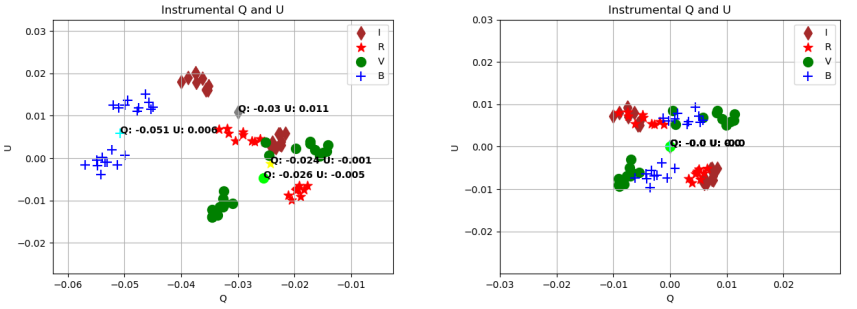

Fig. 19. *Left:* Plot of the Q and U normalized Stokes parameters without the calibration procedure. *Right:* Plot of the Q and U normalized Stokes parameters, calibration procedure implemented. In both cases, the colors represent the measurements in the Johnson filter system. The values in bold font represent the average values of the measurements.

with the OpticStudio and Solidworks programs.

REFERENCES

Bevington, P.R. & Robinson, D.K., 2010, Data reduction and error analysis for the Physical Sciences. Boston: McGraw-Hill.

Clarke, D. 2010, Stellar Polarimetry by David Clarke. Wiley, 2010.

Compain E., Poirier S., & Drevillon B., 1999, Applied Optics 38, 3490-3502. https://doi.org/10.1364/AO.38.003490

Devaraj, R., Luna, A., Carrasco, L., Vázquez-Rodríguez, M. A., Mayya, Y. D., Tánori, J. G., Serrano Bernal, E. O. 2018. PASP, 130, 055002. https://iopscience.iop.org/article/10.1088/1538-3873/aaab3f/meta

Gledhill, T. M., Chrysostomou, A., Hough, J. H., et al. 2001, MNRAS, 322, 321. https://doi.org/10.1046/j.1365-8711.2001.04112.x

Helhel, S., Khamitov, I., Kahya, G. et al., 2015, Exp Astron 39, 595–604. https://doi.org/10.1007/s10686-015-9468-8

TABLE 5

RESULTS OF THE POLARIZED SOURCES OBSERVATIONS.

Object	filter	$P(\%)$	$P_{lit}(\%)$	$A(^\circ)$	$A_{lit}(^\circ)$
HD154445	I	2.975 ± 0.5	3.06	92.679 ± 1.68	91
	R	2.988 ± 0.3	3.6	93.6 ± 1.63	90.1
	V	2.994 ± 1.3	3.72	82.858 ± 2.07	90.3
	B	1.612 ± 0.6	3.44	99.293 ± 4.55	90.1
HD161056	I	3.782 ± 0.8	3.578	71.04 ± 1.41	69.08
	R	4.593 ± 0.6	3.846	75.97 ± 1.12	68.2
	V	4.54 ± 1.01	4.048	60.568 ± 1.52	68.61
	B	4.5 ± 0.8	3.771	68.8 ± 2.0	68.71

Hiltner, W. A. 1949, ApJ, 109, 471. (Paper II) https://articles.adsabs.harvard.edu/full/1949ApJ...109..471H

Howell, S. B. 2006, Handbook of CCD astronomy, 2nd ed., by S.B. Howell. Cambridge observing handbooks for research astronomers, Vol. 5 Cambridge, UK: Cambridge University Press, 2006.

Lazarian, A., & Hoang, T. 2007, MNRAS, 378, 910. https://doi.org/10.1111/j.1365-2966.2007.11817.x

Medina S. 2020, Polarímetro óptico para estudios de cuerpos menores del Sistema Solar. México: Instituto Nacional de Astrofísica, óptica y Electrónica. http://inaoe.repositorioinstitucional.mx/jspui/handle/1009/1995

O'Connor E. 2020. Development of a high-time resolution optical polarimeter for astronomy. Ireland: NUI Galway. https://researchrepository.universityofgalway.ie/entities/publication/fb22fca1-6f8f-400b-a40d-3e0ce7684cf9

Oliva E. 1996, Astron. Astrophys. Suppl. Ser. 123, 589-592. https://doi.org/10.1051/aas:1997175

Patat F. & Romaniello M. 2004, PASP, 118, 146. https://iopscience.iop.org/article/10.1086/497581/meta

Pernechele C., Abe L., Bendjoya P., Cellino A., Massone G., Rivet J. P. & Tanga P., 2015, Proc. of SPIE, 8446, pp. 84462H-1 - 84462H-6. https://doi.org/10.1117/12.925933

Poidvein F., 2023, Departamento de Astronomia. http://astroweb.iag.usp.br/~polarimetria/padroes/index.html

Ritacco A. 2016, Polarimetry at millimeter wavelengths with the NIKA and NIKA2 instruments. France: Université Grenoble Alpes. https://hal.science/tel-01467862v1

Saito T., Sunati T., Kiyono K. & Oikawa T., 2022 J. Phys.: Conf. Ser. 2149 012009. https://dx.doi.org/10.1088/1742-6596/2149/1/012009

Scarrott S. M. & Scarrott R. M. J. 1994, BVRI imaging polarimetry of the Frosty Leo nebula. MNRAS268, 615-624. https://doi.org/10.1093/mnras/268.3.615

Serrano-Bernal E. 2021, The Near-Infrared Polarimeter of Cananea, POLICAN: Optimization, Observations, and Results. México: Instituto Nacional de Astrofísica, óptica y Electrónica.. http://inaoe.repositorioinstitucional.mx/

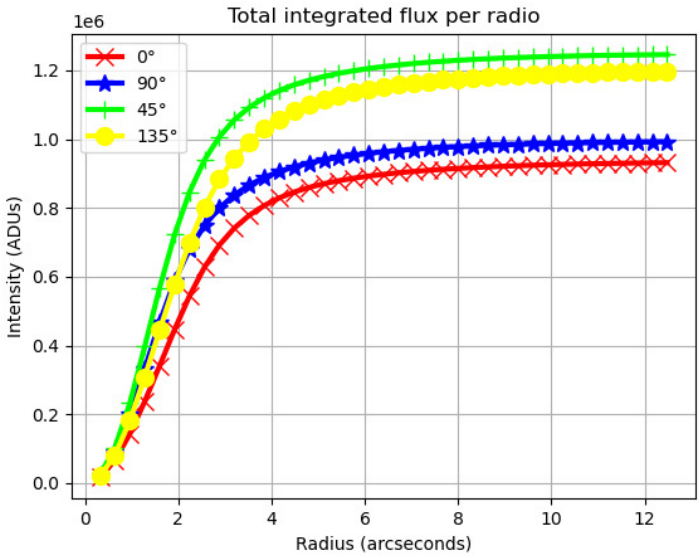

Fig. 20. Growing curve of the flux retrieved at HD 161056 observation. This task aids us in properly computing the polarization fraction and angle values of an observed source. This is implemented in all of the polarimetric standard stars analyses.

jspui/handle/1009/2574

Serrano-Bernal E., Sabin L., Luna A., Devaraj R., Mayya Y. D. & Carrasco L., 2020, MNRAS, 495, 2599-2606. https://doi.org/10.1093/mnras/staa1291

Shurcliff, W. A. 1966, Polarized Light: Production and Use, by William A. Shurcliff, Copyright 1962, 2nd Edition 1966, Reprint 2014. Cambridge: Harvard University.

Tinbergen, J. 1996, Astronomical Polarimetry, by Jaap Tinbergen, pp. 174. Cambridge, UK: Cambridge University Press, September 1996., 174.

A. García-Pérez, A. Luna, J. Castro-Ramos and E. O. Serrano-Bernal: Instituto Nacional de Astrofísica, Óptica y Electrónica. Luis Enrique Erro #1, Sta. María Tonanzintla, 72840 San Andrés Cholula, Pue. (alexgp, aluna, jcastro, arthas@inaoep.mx)

S. Medina: Tyndall National Institute. Lee Maltings Complex Dyke Parade, Cork, Cork, T12 R5CP, Ireland. (s.medina-rangel@mycit.ie)

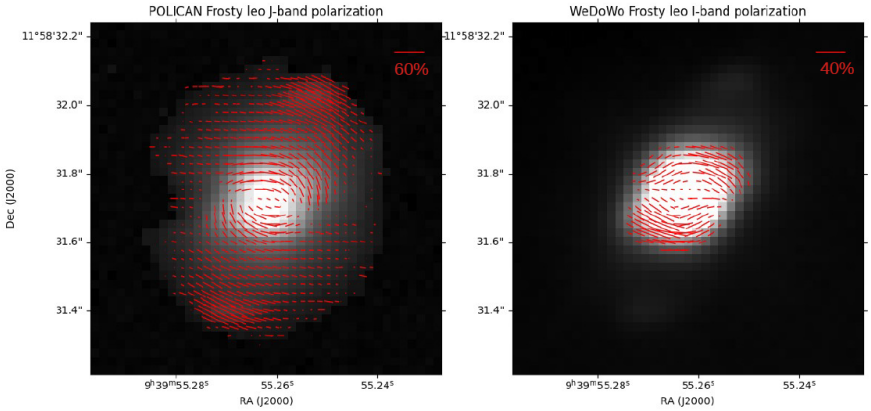

Fig. 21. *Left:* Total intensity results from the Frosty Leo observation at J-band with the polarization vectors over plotted. Performed by the OAGH polarimeter POLICAN as described by Serrano-Bernal et al. (2020). *Right:* Total intensity results from Frosty Leo observation at I-band with the polarization vectors over plotted. Performed by the WeDoWo module on the OAN-TNT telescope.

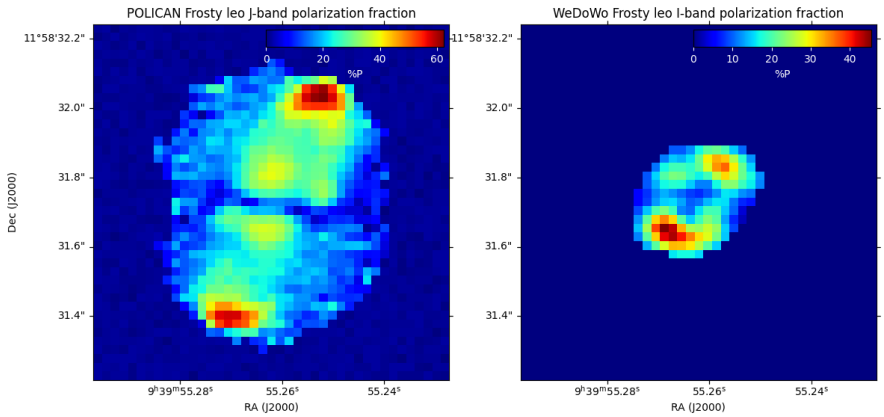

Fig. 22. *Left:* Polarization fraction results from the Frosty Leo observation at J-band. Performed by the OAGH polarimeter POLICAN as described by Serrano-Bernal et al. (2020). *Right:* Polarization fraction results from Frosty Leo observation at I-band. Performed by the WeDoWo module on the OAN-TNT telescope.

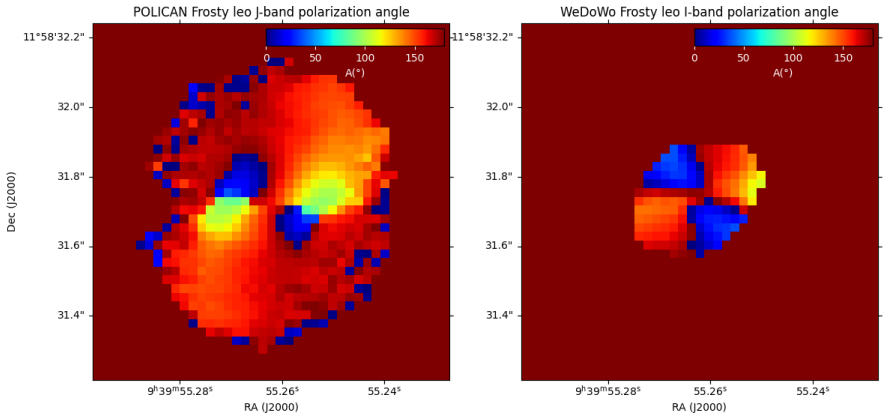

Fig. 23. *Left:* Polarization angle results from the Frosty Leo observation at J-band. Performed by the OAGH polarimeter POLICAN as described by Serrano-Bernal et al. (2020). *Right:* Polarization angle results from Frosty Leo's observation at I-band. Performed by the WeDoWo module on the OAN-TNT telescope.